Organic Electronics 12 (2011) 1826–1834

Contents lists available at SciVerse ScienceDirect

Organic Electronics

journal homepage: www.elsevier.com/locate/orgel

Selective growth and enhanced field emission properties of micropatterned iron phthalocyanine nanofiber arrays

Kuo-Jung Huang [a], Yu-Sheng Hsiao [b,*], Wha-Tzong Whang [a,*]

[a] Department of Materials Science and Engineering, National Chiao Tung University, Hsinchu 30010, Taiwan, ROC
[b] Research Center for Applied Sciences, Academia Sinica, Taipei 11529, Taiwan, ROC

ARTICLE INFO

Article history:
Received 29 April 2011
Received in revised form 15 July 2011
Accepted 17 July 2011
Available online 5 August 2011

Keywords:
Organic nanostructures
Iron phthalocyanine
Field emission
Pattern
Thermal evaporation

ABSTRACT

In this study, we developed a simple method for the micropatterned growth of iron phthalocyanine (FePc) nanofiber arrays using a thermal evaporation process. By controlling the surface energy and the temperature of the substrate (T_{sub}), we obtained FePc films featuring a grain-like (in-plane) morphology on Si surfaces (higher surface energy) and a fiber-like (out-of-plane) morphology on Ag surfaces (lower surface energy) within a certain range of values of T_{sub}. On the Ag surfaces, these temperature-induced FePc nanofibers featured a high aspect ratio (AR) of 30.3 ± 3.6, with a mean length of 699 ± 216 nm and a mean radius of 22.2 ± 4.3 nm, as-prepared at a value of T_{sub} of 240 °C. The FePc films obtained at values of T_{sub} of 25, 120, 180, and 240 °C all possessed α-phase crystalline structures. Because the growth structures of the FePc molecules on the Si and Ag substrates were quite different, we could control the growth of micropatterned 1D FePc nanofiber arrays on previously patterned Ag/Si substrates. From the comparison of the field emission (FE) properties in different ARs of patterned devices, higher AR (30.3 ± 3.6) of devices (**FE-240-P**; T_{sub} of 240 °C) exhibited better FE performance than lower AR (6.0 ± 2.6) of devices (**FE-180-P**; T_{sub} of 180 °C). The FE current density of devices (T_{sub} of 240 °C) increased from 0.13 mA/cm^2 for the unpatterned device (**FE-240-N**) to 6.77 mA/cm^2 for the patterned device (**FE-240-P**) at an applied electric field of 12 V/μm. The turn-on electric fields required to produce a current density of 10 μA/cm^2 were 7.7 and 10.3 V/μm for the patterned and unpatterned FePc emitters, respectively. From the slopes of Fowler–Nordheim plots, we estimated the field enhancement factors (β) of **FE-240-P** and **FE-240-N** to be 314 and 329, respectively. Studies of the emission current stability revealed that the FePc nanofibers possessed outstanding anti-degrading capability. During stability tests, the micropatterned FePc emitter (**FE-240-P**) displayed an efficient emission current with fluctuations of less than 20%. Because this facile platform allows control over the morphologies of films of small organic molecules merely by tuning the surface energy of the substrates, such micropatterned-FePc nanofibers might have great applicability in practical field emitters.

1. Introduction

Because organic electronics based on the π-stacking of organic molecules have unique applications, they have become the focus of intensive research [1–3]. Recently, the self-assembly of several small organic molecules – including tris(8-hydroxyquinolinato)aluminum (Alq_3) [4–7], anthracene, perylene (PY) [8], coronene [9], metal-tetracyanoquinodimethane charge-transfer complexes [10–17],

* Corresponding authors. Tel.: +886 2 27898000x21; fax: +886 2 27826680 (Y.-S. Hsiao), tel.: +886 35 731873; fax: +886 35 724727 (W.-T. Whang).
E-mail addresses: yshsiao@gate.sinica.edu.tw (Y.-S. Hsiao), wtwhang@mail.nctu.edu.tw (W.-T. Whang).

1566-1199/$ - see front matter © 2011 Elsevier B.V. All rights reserved.
doi:10.1016/j.orgel.2011.07.013

metal phthalocyanines (MPcs) [18–22], and 1,5-diaminoanthraquinone [23–25] – has been used to prepare various nanostructures for applications in organic electronics, especially photovoltaic devices and field emitters, with the advantages of low-cost, low-temperature processing and mechanical flexibility. Among those materials, MPcs, which feature a central metal atom bound to a π-conjugated ligand, have particularly attractive properties for their application in optoelectronic devices (e.g., light emitting diodes [26], gas sensors [27–29], field-effect transistors [30–33], solar cells [34–36], and field emission devices [20,21]). Most active layers of MPcs have been fabricated using deposition methods, including organic vapor-phase deposition (OVPD) [1,18,37,38], thermal evaporation [19,21], and molecule beam epitaxy (MBE) [39]. It has been reported [1,21,22,25] that the morphologies of thin films of MPcs depend on the type of deposition technique, the heat-treatment temperature, and the conditions of the substrates during the deposition process. Tuning these various growth conditions can have a dramatic effect on the resulting morphologies and electronic properties, thereby requiring further investigation of the potential use of such structures in optoelectronic devices.

When developing field emitters, the inter-fiber distance, the aspect ratio, and the density of the nanofibers are theoretically and experimentally important parameters for achieving efficient field emission (FE) performance. Under practical conditions, however, it can be difficult to control the inter-fiber distance at an ideal fiber density. Although higher-density nanofibers provide higher electron currents, electrostatic screening effects are observed in such films; therefore, high-density nanofiber films do not possess appropriate FE properties [40]. To decrease the screening effect, forming a pattern array of aligned nanofibers is a facile method of enhancing FE properties [41]. Moreover, a recent study found that the electric field gradient at the edge of an emission bundle is significantly higher than that at its center [42]. Therefore, the ability to design patterns of nanofiber films should allow efficient increases in FE performance.

In this present study, we used FePc as a starting material, instead of a precursor of the catalyst for CNT growth [43], to fabricate FePc nanostructures on Si and Ag substrates. Because the surface energy and temperature of a substrate are both important factors affecting the morphologies of FePc films, we sought appropriate conditions for the direct growth of FePc films featuring planar structures on Si surfaces (higher surface energy) and fiber-like structures on Ag surfaces (lower surface energy). We used scanning electron microscopy (SEM) and high-resolution transmission electron microscopy (HRTEM) to characterize these 1D FePc nanofiber films. By taking advantage of such selective growth at various substrate temperatures, we used micropatterned Ag/Si substrates to obtain the fine growth of FePc nanofibers on the patterned Ag regions and in-plane FePc structures on the remaining open areas of the Si surfaces. To study the enhancement in FE performance when using field emitters with such micropatterned geometries, we used a vacuum emission measurement (VEM) system to compare the FE characteristics and device stability tests relative to those of corresponding unpatterned devices.

2. Experimental details

FePc thin films were deposited using a thermal evaporator operated at a base pressure of 7×10^{-6} torr. A commercially available FePc powder (purity: 96%; Tokyo Chemical Industry) was used as received without further purification; it was sublimed onto two kinds of substrates (Si and Ag). The Ag substrates were prepared by depositing Ag films onto Si (1 0 0) substrates using an electron beam (e-beam) evaporator. Prior to e-beam evaporation of the Ag film, a Ti layer (thickness: 300 Å) was deposited on a cleaned Si substrate as an adhesion layer. Without breaking the vacuum, a thin layer of Ag (thickness: 1000 Å) was then deposited. The influence of the substrate temperature (T_{sub}) on the FePc film morphology during FePc thermal evaporation was tested at values of T_{sub} of 25, 120, 180, and 240 °C. The sublimation of the FePc powder was performed at a crucible temperature of 180 °C; the corresponding deposition rate, controlled by a quartz crystal microbalance, was 0.4 Å/s.

Top and cross-sectional views of the morphologies of the FePc thin films were investigated using a JEOL JSM-6500F scanning electron microscope. The profiles and fine structure of nanofibers were imaged and analyzed using a JEOL-2010 high-resolution transmission electron microscope. The phase and crystallinity of the FePc nanofibers were characterized using grazing-incidence X-ray diffraction (GIXRD), employing a Bruker D8 system with Cu Kα radiation. The incident angle of the X-ray beam was fixed at 0.2°. Contact angles and surface energies were determined on each substrate using a Krüss universal surface tester (model GH-100), the geometric mean approximation, and three standard liquids: water (H_2O), diiodomethane (CH_2I_2), and ethylene glycol [$C_2H_4(OH)_2$]. The surface energies of the substrates were measured using the Owens and Wendt method. The valence band [highest occupied molecular orbital (HOMO)] of the FePc materials was surveyed using photoelectron spectroscopy in air (PESA; AC-2 photoelectron spectrometer); the Riken Keiki apparatus detected the number of photo-emitted electrons per second (CPS) as a function of the photon energy, using a UV light source for excitation and a gas-flow Geiger counter. The relationship between CPS and the photon energy is described using the approximate equation [44]:

$$\mathrm{CPS}^{1/2} = \frac{M}{k}(h\nu - \phi) \quad (1)$$

where M is an emission constant, k is the Boltzmann constant, $h\nu$ is the photon energy, and ϕ is the work function. When the surface materials were bombarded under a gradually increasing amount of UV light, photoelectrons were emitted from the surface (from a depth of several to hundred angstroms) at a certain energy level, due to the photoelectron effect. These emitted photoelectrons were then counted by a detector and open counter. The value of ϕ was determined through linear extrapolation of $\mathrm{CPS}^{1/2}$ to zero yield [44], when the PESA data were fitted using the software supplied with the spectrometer. UV–Visible (UV–Vis) spectra (300–1100 nm) were recorded using a Shimadzu UV-3600 spectrophotometer.

The FE characteristics of the FePc nanofibers were determined using a VEM system under a base pressure of 5×10^{-6} torr. Indium tin oxide (ITO) plate glasses were used as anodes, positioned above the substrate surfaces at a distance of 60 μm. The FE instrument featured a plate-to-plate geometry; the active area of the FePc nanofibers was 0.06 cm^2 for the unpatterned devices and 0.006156 cm^2 for the micropatterned devices featuring 171 (19×9) squares, each with a width of 60 μm. Current density–electric field (J–E) curves of the FE devices were measured using a Keithley 237 instrument (accuracy: 10^{-13} A). The emission currents of the FePc nanofibers were monitored as a function of the sweep bias. Stability tests were performed for 3000 s under a constant applied field of 11 V/μm at room temperature. The patterned FE devices are denoted herein as "**FE-X-P**," where **X** refers to the FePc nanofiber films were prepared at the value of T_{sub}. In addition, the unpatterned FE devices are denoted as "**FE-X-N**".

3. Results and discussion

The growth mechanisms of organic thin films on substrates are complicated because of specific issues related to each type of organic molecule; for example, the effects of the surface energy of the substrate, noncovalent interactions at the molecule–substrate interface, and intermolecular forces between molecules. Stranski–Krastanov growth tends to be the mode most frequently observed for small organic molecules under thermal evaporation conditions [45]. Previous studies [21,34–36] have revealed that the surface energy and substrate temperature are both important factors controlling the morphologies of films of small organic molecules. Therefore, in this study, we selected Ag and Si, with surface energies of 34.8 and 41.3 mJ/m^2, respectively, as electrodes for the selective growth of micropatterned FePc nanofiber films for FE applications. Fig. 1 displays SEM images of the FePc films deposited on the Si and Ag substrates at various values of T_{sub}. At a value of T_{sub} of 25 °C, all of the FePc thin films on the Si and Ag substrates exhibited analogous and contiguous granular crystals with smooth morphologies [Fig. 1(A, E, and I)]. When we increased the value of T_{sub} from 120 to 240 °C, elongated FePc grain-like films were formed with the in-plane morphology on the Si surface [Fig. 1(B–D)]. In contrast, when the FePc layers were deposited on the Ag substrate at values of T_{sub} in the range 120–240 °C, we obtained high-quality FePc fiber-like films featuring out-of-plane 1D nanostructural morphologies [Fig. 1(F–H) (top-view) and (J–L) (cross-sectional view)]. Notably, we found a high-density of aligned FePc nanofibers in the films deposited on the Ag surface at a value of T_{sub} of 240 °C [Fig. 1(H, L)]. The variation in FePc morphology that occurred upon increasing the value of T_{sub} can be explained by considering the following equation [46]:

$$\gamma_s = \gamma^0[1 - (T_s/T_c)]^n \quad (2)$$

where γ_s is the surface energy at the substrate temperature T_s and γ^0 is the surface energy at the critical temperature (T_c); the value of n may be close to unity for cathodes. This formula suggests that the surface energy of the substrate (γ_s) decreases as the substrate temperature increases, thereby favoring the desorption and surface diffusion of FePc molecules. A decrease in surface energy weakens the molecule–substrate interactions, causing the molecule–molecule interactions (i.e., π–π and van der Waals interactions) to become dominant. When nonpolar molecules (e.g., Alq_3, PY, coronene) form 1D nanofibers, molecular stacking occurs mainly through π–π and van der Waals interactions. In the 1D nanostructure of the stacked planar FePc molecules, we suspect that both face-to-face (π stacking) and edge-to-edge (van der Waals interaction) intermolecular forces play an important role in the 1D self-assembly of the stacking molecules [4–9].

At the device level of field emitters, the field enhancement factor (β) is approximated by the aspect ratio (AR; length-to-radius ratio) of a 1D nanostructure, defined as AR = (mean length; L)/(mean radius; r_m). A 1D nanostructure having a higher AR will exhibit a larger geometrical field enhancement and a lower turn-on field [47]. In this study, we found that changing the deposition time adjusted the lengths of the nanofibers. Besides, both high-density and high-AR of aligned FePc nanofiber films can be easily achieved on the Ag surface at a value of T_{sub} of 240 °C. To further investigate the influence of AR effect on FE properties, we prepared FePc nanofiber films with different ARs by changing values of T_{sub} of 180 and 240 °C [Fig. 2(A and E)]. Furthermore, the histograms of the fiber length, radius, and AR [Fig. 2(B and F), (C and G), and (D and H)] were obtained for comparison, respectively, which were based on the cross-sectional SEM images of those structures. In the fabrication condition of T_{sub} of 180 and 240 °C, the values of L of these FePc nanofibers with an apparent difference were found to be 124 ± 41 and 699 ± 216 nm, while the values of r_m of these FePc nanofibers were analogous to be 21.9 ± 4.0 and 22.2 ± 4.3 nm, respectively. In addition, the mean values of ARs of individual FePc nanofibers were calculated to be 6.0 ± 2.6 and 30.3 ± 3.6, respectively.

Fig. 3(A) displays a TEM image and the corresponding selected area electron diffraction (SAED) pattern of a single FePc nanofiber, which we had deposited on the Ag substrate at a value of T_{sub} of 240 °C. The TEM image of this FePc nanofiber exhibits fringes, suggesting that the FePc molecules were stacked in short-range order at the edges of the nanofiber, but entangled randomly within the nanofiber. The SAED pattern presented in the inset indicates that the FePc nanofibers were polycrystalline. From studies of several polymorphs of phthalocyanine materials, it is well established that the processing conditions can result in different phase formations (e.g., polymorphs of α and β phases), which exhibit slightly different structural and electrical characteristics [18]. The structural difference between these two polymorphs is the tilt angle of the molecular plane with respect to the stacking b-axes, with the tilt angle of the α phase being smaller than that of the β phase [39]. In addition, the α-form of a FePc film can transform to the β-form during subsequent annealing or when deposited at higher temperature [48,49]. Fig. 3(B) presents GIXRD patterns of commercial FePc powders and the FePc thin films that we deposited on the Ag surface at various

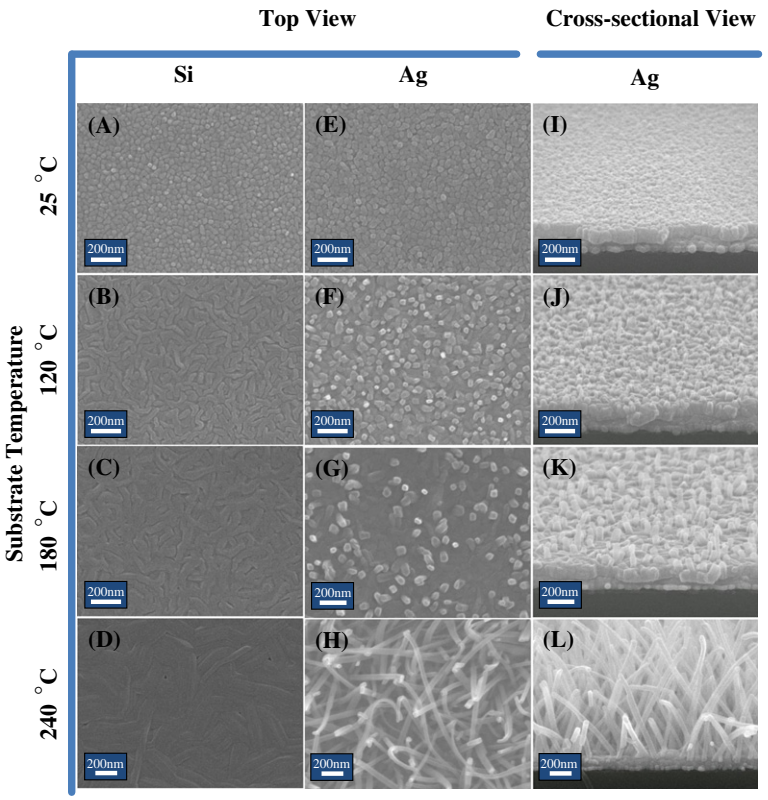

Fig. 1. Top-view and cross-sectional SEM images of FePc thin films deposited on Si and Ag substrates at values of T_{sub} of 25 (A, E, and I), 120 (B, F, and J), 180 (C, G, and K), and 240 °C (D, H, and L).

values of T_{sub}. The commercial FePc powders were crystalline in character; a single peak appeared at a value of 2θ of 6.96°, corresponding to the (2 0 0) peak of the α-FePc phase. The diffraction patterns of the thin films deposited on the Ag substrate at a value of T_{sub} of 25 °C suggested that they featured the same polymorphs as those deposited on sapphire at the same temperature [39]. The absence of diffraction patterns of the β-FePc phase (peaks at 7.01° and 9.6°) [39] suggested that the structure of the FePc nanofibers deposited on the Ag surfaces at a value of T_{sub} of 240 °C was that of the α phase, with preferential orientation along the (2 0 0) direction.

To further understand the energy levels of the FePc materials for FE applications, we used photoelectron spectroscopy [Fig. 4(A)] and UV–Vis spectroscopy [Fig. 4(B)] to measure the HOMO energy levels and obtain the energy gap. Using the supplied software, we fitted the PESA data through linear extrapolation of the value of $CPS^{1/2}$ to zero yields, obtaining a HOMO energy level for FePc of 5.01 eV relative to the vacuum level. The Q-band in Fig. 4(B), between 500–800 nm in the UV–Vis spectrum of the FePc films, revealed overlapping of the three main bands with maxima at 570, 630, and 710 nm. From the onset wavelength at 817 nm, we derived the energy gap and LUMO energy level for the FePc materials of 1.52 and 3.49 eV. Fig. 4(C) displays a schematic representation of the energy level diagram; the work function of the Ag cathode substrate was 4.8 eV. Therefore, electrons injected from the Ag substrate into the LUMO of the FePc materials would have to conquer an energy gap of 1.31 eV.

Next, we performed the selective growth of micropatterned FePc nanofiber arrays on the patterned Ag/Si substrates. In this electrode system, the Ag region would induce the formation of the fiber-like structure of FePc and the Si region would result in the flat grain-like structure. We prepared the patterned Ag substrate in three steps: (i) First, a purpose-made shadow mask was placed on the surface of Si substrate [Fig. 5(A and B)]. The pattern of this purpose-made mask featured a total of 171 (19×9) squares, each with a width of 60 μm. The active area of the device was 0.006156 cm^2. (ii) Next, 100-nm-thick Ag films were deposited on the substrate through e-beam evaporation [Fig. 5(C)]. (iii) Finally, the FePc nanofiber arrays were formed at a certain substrate temperature via thermal evaporation [Fig. 5(D)]. Fig. 6(A–D) display top-view and cross-sectional SEM images of the FePc thin films deposited on the patterned Ag substrate at 240 °C. In Fig. 6(B–C), it is evident that the vertical growth of nanofibers was restricted to the areas presenting the Ag film, where the pattern of the cathode featured nanofiber arrays with each square having a width of 60 μm and an interval of 45 μm between neighboring squares. From the point of view of practical applications, the fabrication of FePc nanofiber arrays on patterned Ag substrates at low temperature (<250 °C) through simple patterning method should be suitable for developing electronic devices. Fig. 6(D) pro-

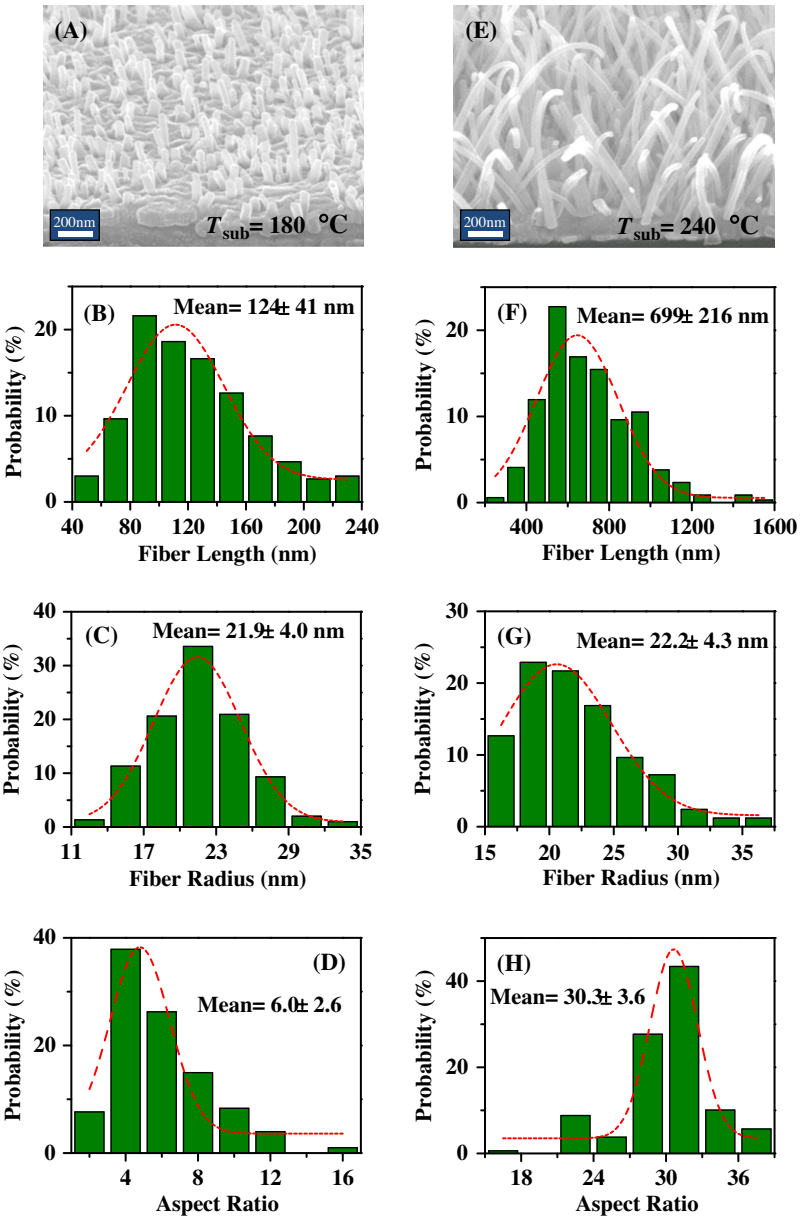

Fig. 2. Cross-sectional SEM images and histograms of FePc nanofiber films deposited on Ag substrates at values of T_{sub} of 180 (A–D) and 240 °C (E–H). Histograms of (B and F) fiber length, (C and G) fiber radius, and (D and H) aspect ratio of these two FePc nanofiber films.

vides a tilted-view, magnified SEM image of a FePc film grown on a region between Ag square patterns.

We examined the FE properties of the FePc nanofiber devices using a parallel-plate configuration with a spacing of 60 μm in a vacuum chamber under a pressure of 5×10^{-6} torr. The anode (ITO glass) was connected to the source monitor unit (SMU) of a Keithley 237 instrument; the cathode of the Ag substrate beneath the FePc nanofibers was grounded. We measured the emission current while increasing the applied voltage from 0 to 720 V with a sweep step of 20 V. To investigate the AR effect of FE properties, we examined the FE characteristics (J–E curve) of the patterned FePc nanofiber devices prepared at values of T_{sub} of 180 (**FE-180-P**) and 240 °C (**FE-240-P**), as shown in Fig. 7(A and B). The turn-on fields (defined as the applied field required for a current density of 10 μA/cm^2) of these patterned FE devices were 10 and 7.7 V/μm, respectively; at an applied field of 12 V/μm, the maximum current densities were 0.26 and 6.77 mA/cm^2, respectively. The Fowler–Nordheim (FN) equation describes the dependence of the emission current of a field emitter on the applied field [50]:

$$\ln\left(\frac{J}{E^2}\right) = \ln\left(\frac{A\beta^2}{\phi}\right) + \left(\frac{-B\phi^{3/2}}{\beta}\right)\left(\frac{1}{E}\right) \quad (3)$$

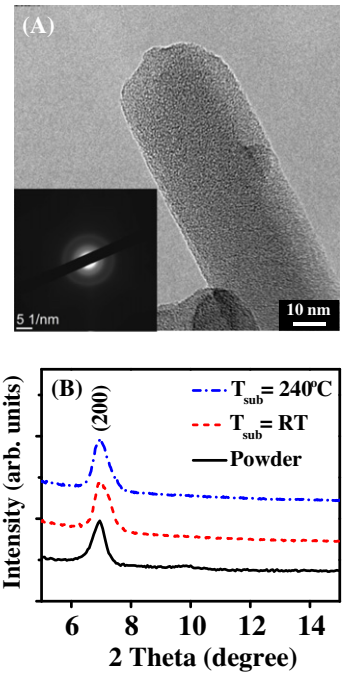

Fig. 3. (A) HRTEM image of FePc nanofibers formed on a Ag substrate; inset: corresponding SAED pattern; (B) XRD patterns of FePc commercial powder and thin films deposited on Ag surfaces at values of T_{sub} of 25 and 240 °C.

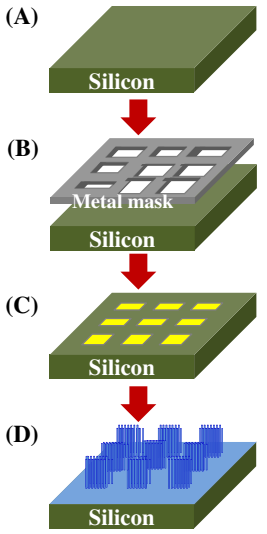

Fig. 5. Flow chart of the growth of micropatterned FePc nanofiber arrays: (A) a P-type Si (1 0 0) wafer (heavy doped); (B) a purpose-made metal mask for Ag layer deposition using an e-beam evaporator; (C) the resulting patterned Ag arrays; (D) the well-aligned FePc nanofibers grown selectively on the patterned Ag arrays through thermal deposition.

where A and B are constants (1.54×10^{-6} A eV/V^2 and 6.83×10^3 V/eV$^{3/2}$/μm, respectively), J is the current density, E is the applied field, and ϕ is the local work function of the emitter material. By plotting $\ln(J/E^2)$ with respect to $1/E$, the slope of the line of best fit can be used to deduce the field enhancement factor (β):

$$\beta = -\frac{6.83 \times 10^3 \phi^{3/2}}{S} \tag{4}$$

where S is the slope of the FN plot. The linear FN plots of **FE-180-P** and **FE-240-P** reveal that the J–E characteristics of the FePc nanofibers followed the FN field emission mechanism, indicating that cold electrons tunneled

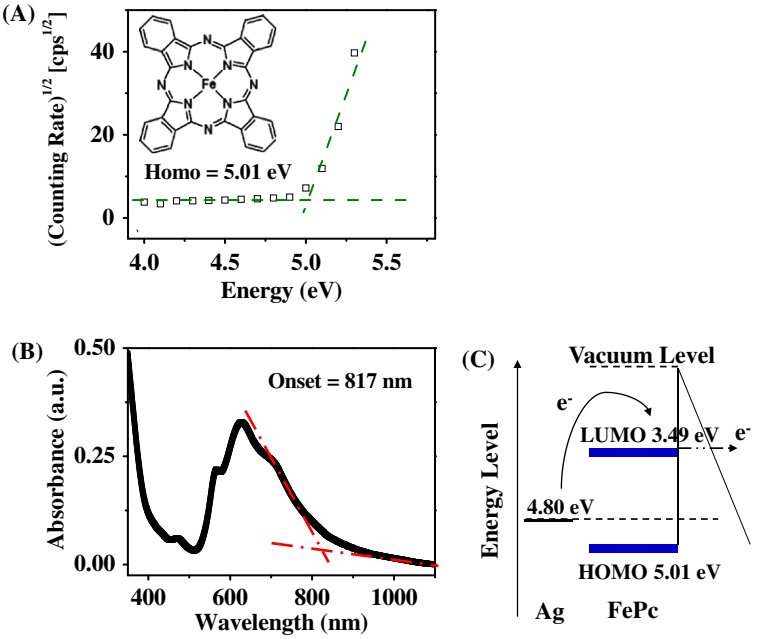

Fig. 4. (A) PESA analysis of the FePc thin films. Inset: molecular structure of FePc. (B) UV–Vis absorption spectra of the FePc thin films. (C) Schematic representation of the energy levels and electrons field-emitting through the FePc nanofibers.

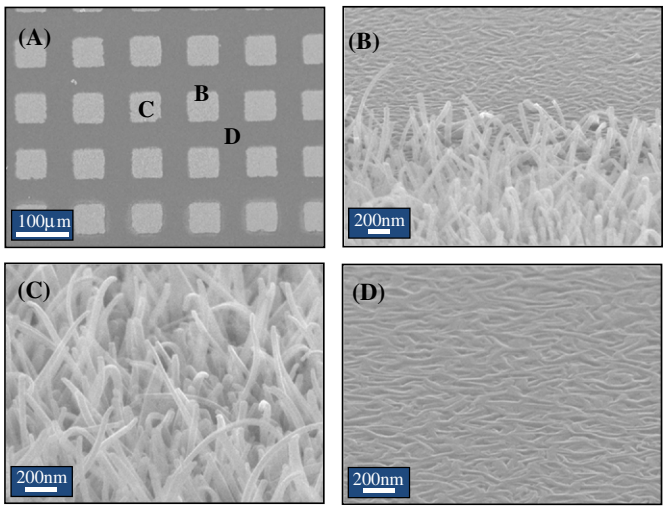

Fig. 6. (A) Top-view SEM images of (A) patterned FePc nanofiber arrays. (B–D) Higher-magnification tilted-view images of (B) the margin of the patterned nanofibers grown on the substrate, (C) the patterned square, and (D) the FePc thin films grown on the Si region in the absence of a Ag layer.

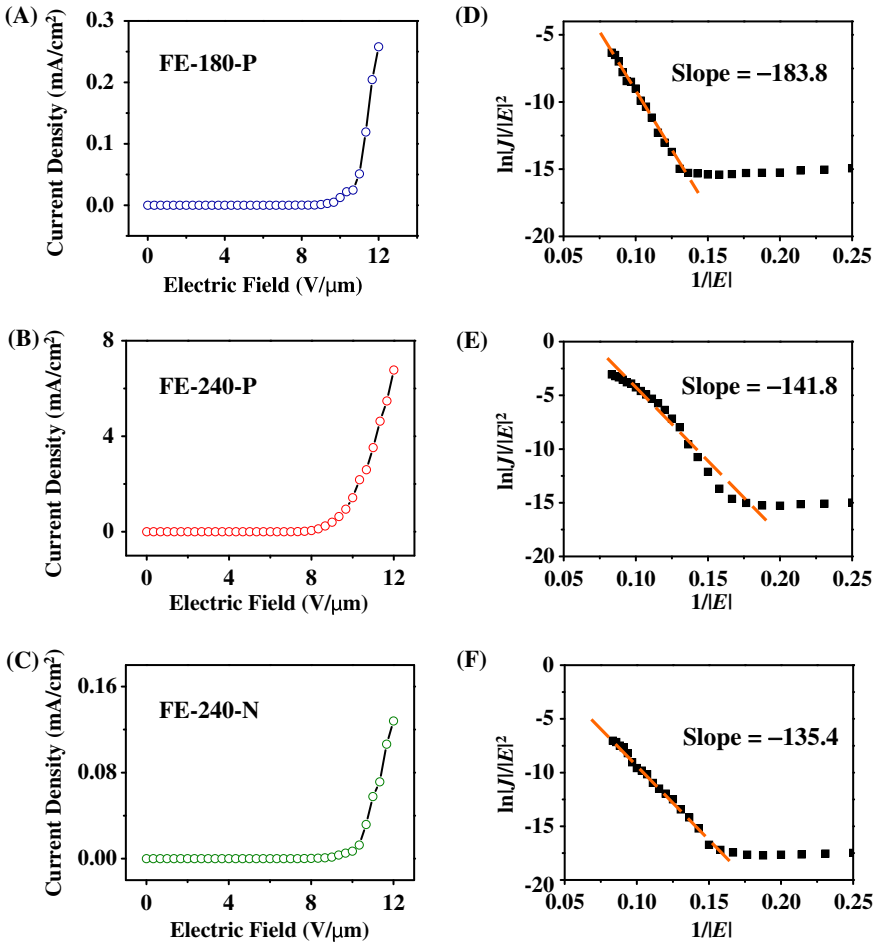

Fig. 7. Field emission *J*–*E* curves and corresponding FN plots of (A and D) **FE-180-P**, (B and E) **FE-240-P**, and (C and F) **FE-240-N**.

through the quantum energy barrier (i.e., quantum tunneling process) under an applied field [Fig. 7(D and E)]. The slopes of the FN plots for **FE-180-P** and **FE-240-P** were −183.8 and −141.8, respectively. Because the LUMO en-

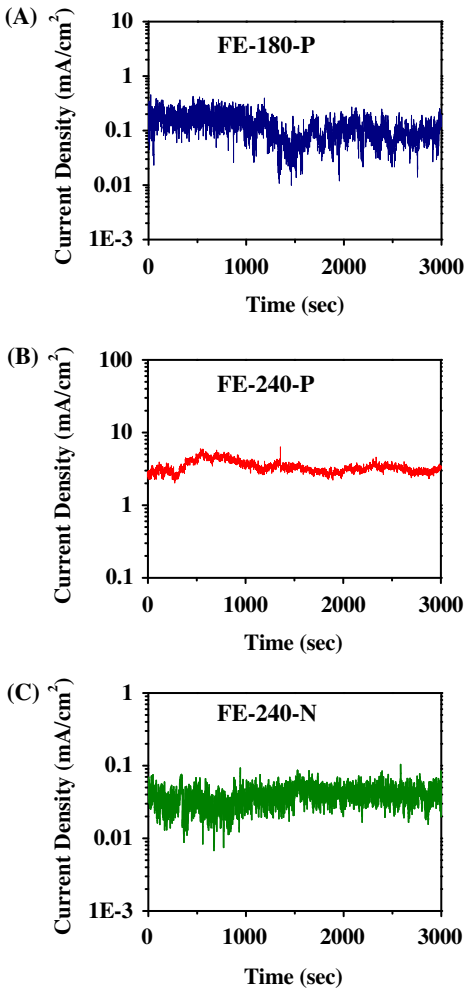

Fig. 8. Emission current stability plots of (A) **FE-180-P**, (B) **FE-240-P**, and (C) **FE-240-N** recorded for 3000 s under a constant applied field.

ergy level (ϕ) of FePc was 3.49 eV, we estimated the values of β of these patterned FE devices to be 242 and 314, respectively. According to FN theory, β is strongly dependent on the geometric structure [51–54] (i.e., shape, size, alignment, crystallinity, AR) and density of the nanofibers grown on the cathode. In our system, **FE-240-P** exhibited efficient FE performance, in terms of a lower turn-on field, higher emission current and larger value of β, relative to that of **FE-180-P**, suggesting the higher AR of patterned devices were suitable for the FE application. To study the enhancement of patterned geometries in FE performance, we also performed the FE measurements of the unpatterned FePc nanofiber devices prepared at 240 °C (**FE-240-N**) as a reference. In the Fig. 7(C), the turn-on field of **FE-240-N** was 10.3 V/μm, and the maximal current density of that was 0.13 mA/cm^2 at an applied field of 12 V/μm. Fig. 7(F) reveals the slope of the linear FN plot for **FE-240-N**, getting that the value of β of **FE-240-N** was approximately 329. Notably, the maximal current density of **FE-240-P** was over 50 times greater than that of **FE-240-N**; that is to say, its FE properties had obviously improved. When the number-density of the nanofibers in each square pattern is sufficiently high [41], the individual nanofiber can be replaced by the square pattern, which can be considered as a single emitter in FE fabrication. In this study, the patterned FePc nanofiber arrays exhibited enhanced emission characteristics that resulted from the pattern design decreasing the screening effect [40]. Each FePc nanofiber square pattern could be regarded as an independent field emitter. Moreover, each individual FePc nanofiber square pattern, as an isolated emitter, allows the emission of electrons from the edges of the square pattern. The highly efficient FE current can be attributed to the edge effect at a certain level [42].

We performed stability tests of our aligned FePc nanofibers for 3000 s under an applied field of 11 V/μm at room temperature. Fig. 8 presents the plots of the FE current density versus testing time for **FE-180-P**, **FE-240-P**, and **FE-240-N**. The calculated mean current density was ca. 0.12 mA/cm^2 for **FE-180-P** [Fig. 8(A)], ca. 3.39 mA/cm^2 for **FE-240-P** [Fig. 8(B)], and ca. 0.04 mA/cm^2 for **FE-240-N** [Fig. 8(C)]. Particularly, **FE-240-P** exhibited remarkably stable emission current with fluctuations of less than 20%. Furthermore, we observed slowly increasing emission currents from all emitters over time. Relative to other organic FE devices [5,20,21], the comparable properties of the FePc nanofibers prepared at a low fabrication temperature and exhibiting a low turn-on field suggest their potential application in organic field emitters. The pattern design of the well-aligned 1D FePc nanostructures has advantages over other nanomaterials in that it allows FE improvement. Thus, this promising organic nanomaterial sustained a stable FE current, without any decay, during the measurement period, demonstrating that the patterned FePc nanofiber arrays, prepared at the value of T_{sub} of 240 °C, have great applicability for use in cold field electron-emitting devices.

4. Conclusions

By varying the surface energy and the temperature of the substrates during vacuum evaporation, the morphology of self-assembled FePc films can be controlled to form in-plane structures on Si surfaces (higher surface energy) and out-of-plane structures on Ag surfaces (lower surface energy). These temperature-enhanced and well-aligned 1D FePc nanofibers exhibited FE characteristics and followed FN behavior. Using such morphological control, we grew the patterned FePc nanofibers selectivity on previously patterned Ag/Si substrates; moreover, the higher AR of the patterned device (**FE-240-P**) exhibited better FE performance than **FE-180-P**. In the optimal growth condition of T_{sub} of 240 °C, the emission current of the device improved dramatically from 0.13 mA/cm^2 for the unpatterned device to 6.77 mA/cm^2 for the patterned device (when biased at an applied field of 12 V/μm), while the turn-on electric field of the device decreased accordingly from 10.3 to 7.7 V/μm. In FE stability tests, the current densities of **FE-240-P** exhibited fluctuations of less than 20%, revealing its stable and superior property within the duration of the measurement process. The enhanced FE performance and the stability of the emission current sug-

gest that this facile method for fabricating patterned FePc nanofiber arrays is suitable for their application in electron-emitting devices.

Acknowledgment

We thank for National Science Council of Taiwan, ROC, for financial support (project NSC 97-2221-E-009-012-MY3).

References

[1] A.B. Djurišić, A.M.C. Ng, K.Y. Cheung, M.K. Fung, W.K. Chan, Journal of Materials Science and Technology 24 (2008) 563.
[2] Y.S. Zhao, H. Fu, A. Peng, Y. Ma, D. Xiao, J. Yao, Advanced Materials 20 (2008) 2859.
[3] Y.S. Zhao, H. Fu, A. Peng, Y. Ma, Q. Liao, J. Yao, Accounts of Chemical Research 43 (2010) 409.
[4] J.J. Chiu, C.C. Kei, T.P. Perng, W.S. Wang, Advanced Materials 15 (2003) 1361.
[5] C.P. Cho, T.P. Perng, Organic Electronics 11 (2010) 115.
[6] W. Chen, Q. Peng, Y. Li, Advanced Materials 20 (2008) 2747.
[7] Y.S. Zhao, C. Di, W. Yang, G. Yu, Y. Liu, J. Yao, Advanced Functional Materials 16 (2006) 1985.
[8] H. Liu, Y. Li, S. Xiao, H. Gan, T. Jiu, H. Li, L. Jiang, D. Zhu, D. Yu, B. Xiang, Y. Chen, Journal of the American Chemical Society 125 (2003) 10794.
[9] S.C. Suen, W.T. Whang, B.W. Wu, Y.F. Lai, Applied Physics Letters 84 (2004) 3157.
[10] H. Liu, Q. Zhao, Y. Li, Y. Liu, F. Lu, J. Zhuang, S. Wang, L. Jiang, D. Zhu, D. Yu, L. Chi, Journal of the American Chemical Society 127 (2005) 1120.
[11] S. Cui, Y. Li, Y. Guo, H. Liu, Y. Song, J. Xu, J. Lv, M. Zhu, D. Zhu, Advanced Materials 20 (2008) 309.
[12] F. Tian, W. Liu, C.R. Wang, Journal of Physical Chemistry C 112 (2008) 8763.
[13] H. Liu, X. Wu, L. Chi, D. Zhong, Q. Zhao, Y. Li, D. Yu, H. Fuchs, D. Zhu, Journal of Physical Chemistry C 112 (2008) 17625.
[14] C. Ouyang, Y. Guo, H. Liu, Y. Zhao, G. Li, Y. Li, Y. Song, Y. Li, Journal of Physical Chemistry C 113 (2009) 7044.
[15] H. Liu, Z. Liu, X. Qian, Y. Guo, S. Cui, L. Sun, Y. Song, Y. Li, D. Zhu, Crystal Growth & Design 10 (2010) 237.
[16] K. Zheng, X. Li, X. Mo, G. Chen, Z. Wang, G. Chen, Applied Surface Science 256 (2010) 2764.
[17] C. Ye, K. Zheng, W. You, G. Chen, Nanoscale Research Letters 5 (2010) 1307.
[18] W.Y. Tong, A.B. Djurišić, M.H. Xie, A.C.M. Ng, K.Y. Cheung, W.K. Chan, Y.H. Leung, H.W. Lin, S. Gwo, Journal of Physical Chemistry B 110 (2006) 17406.
[19] S. Karan, B. Mallik, Journal of Physical Chemistry C 111 (2007) 7352.
[20] W.Y. Tong, Z.X. Li, A.B. Djurišić, W.K. Chan, S.F. Yu, Materials Letters 61 (2007) 3842.
[21] S.C. Suen, W.T. Whang, F.J. Hou, B.T. Dai, Organic Electronics 7 (2006) 428.
[22] W.Y. Tong, A.B. Djurišić, A.M.C. Ng, W.K. Chan, Thin Solid Film 515 (2007) 5270.
[23] Y.S. Zhao, J. Wu, J. Huang, Journal of the American Chemical Society 131 (2009) 3158.
[24] Y.S. Zhao, P. Zhan, J. Kim, K. Sun, J. Huang, ACS Nano 4 (2010) 1630.
[25] K.J. Huang, Y.S. Hsiao, W.T. Whang, Organic Electronics 12 (2011) 686.
[26] J. Blochwitz, M. Pfeiffer, T. Fritz, K. Leo, Applied Physics Letters 73 (1998) 729.
[27] M. Bouvet, Analytical and Bioanalytical Chemistry 384 (2006) 366.
[28] T. Nagasawa, K. Murakami, K. Watanabe, Molecular Crystals and Liquid Crystals 316 (1998) 389.
[29] M.I. Newton, T.K.H. Starke, M.R. Wills, G. McHale, Sensors and Actuators B-Chemistry 67 (2000) 307.
[30] J. Zhang, H. Wang, X. Yan, J. Wang, J. Shi, D. Yan, Advanced Materials 17 (2005) 1191.
[31] R.W.I. de Boer, A.F. Stassen, M.F. Craciun, C.L. Mulder, A. Molinari, S. Rogge, A.F. Morpurgo, Applied Physics Letters 86 (2005) 262109.
[32] J. Wang, H. Wang, X. Yan, H. Huang, D. Yan, Applied Physics Letters 87 (2005) 093507.
[33] Q. Tang, H. Li, M. He, W. Hu, C. Liu, K. Chen, C. Wang, Y. Liu, D. Zhu, Advanced Materials 18 (2006) 65.
[34] F. Yang, M. Shtein, S.R. Forrest, Journal of Applied Physics 98 (2005) 014906.
[35] F. Yang, M. Shtein, S.R. Forrest, Nature Materials 4 (2005) 37.
[36] Y.S. Hsiao, W.T. Whang, S.C. Suen, J.Y. Shiu, C.P. Chen, Nanotechnology 19 (2008) 415603.
[37] J.W. Chung, B.K. An, J.W. Kim, J.J. Kim, S.Y. Park, Chemical Communications (2008) 2998.
[38] Y.S. Zhao, D. Xiao, W. Yang, A. Peng, J. Yao, Chemistry of Materials 18 (2006) 2302.
[39] A.K. Debnath, S. Samanta, A. Singh, D.K. Aswal, S.K. Gupta, J.V. Yakhmi, S.K. Deshpande, A.K. Poswal, C. Sürgers, Physica E: Low-dimensional Systems and Nanostructures 41 (2008) 154.
[40] L. Nilsson, O. Groening, C. Emmenegger, O. Kuettel, E. Schaller, L. Schlapbach, H. Kind, J.-M. Bonard, K. Kern, Applied Physics Letters 76 (2000) 2071.
[41] M. Katayama, K.Y. Lee, S.I. Honda, T. Hirao, K. Oura, Japan Journal of Applied Physics 43 (2004) L774.
[42] S. Fujii, S.I. Honda, H. Machida, H. Kawai, K. Ishida, M. Katayama, Applied Physics Letters 90 (2007) 153108.
[43] S. Huang, A.H.W. Mau, Applied Physics Letters 82 (2003) 796.
[44] T. Sakurai, Y. Momose, K. Nakayama, E.-J. Surf, Science Nanotechnology 3 (2005) 179.
[45] J.A. Venables, G.D.T. Spiller, M. Hanbücken, Reports on Progress in Physics 47 (1984) 399.
[46] A.W. Adamson, Physical Chemistry of Surfaces, 5th ed., John Wiley & Sons Publishers, 1990, pp. 55.
[47] F.G. Tarntair, C.Y. Wen, L.C. Chen, J.J. Wu, K.H. Chen, P.F. Kuo, S.W. Chang, Y.F. Chen, W.K. Hong, H.C. Cheng, Applied Physics Letters 76 (2000) 2630.
[48] S.I. Shihub, R.D. Gould, Thin Solid Films 290–291 (1996) 390.
[49] P. Ballirano, R. Caminiti, C. Ercolani, A. Maras, M.A. Orru, Journal of the American Chemical Society 120 (1998) 12798.
[50] R. Fowler, L.W. Nordheim, Proceedings of the Royal Society of London 119 (1928) 173.
[51] Y.W. Zhu, H.Z. Zhang, X.C. Sun, S.Q. Feng, J. Xu, Q. Zhao, B. Xiang, R.M. Wang, D.P. Yu, Applied Physics Letters 83 (2003) 144.
[52] J. Chen, S.Z. Deng, N.S. Xu, S.H. Wang, X.G. Wen, S.H. Yang, C.L. Yang, J.N. Wang, W.K. Ge, Applied Physics Letters 80 (2002) 3620.
[53] B.Y. Li, Y. Bando, D. Golberg, K. Kurashima, Applied Physics Letters 81 (2002) 5048.
[54] C.J. Lee, T.J. Lee, S.C. Lyu, Y. Zhang, H. Ruh, H.J. Lee, Applied Physics Letters 81 (2002) 3648.